Navigating the Fitness Landscapes of Plasmodium falciparum Dihydrofolate Reductase: Evolutionary Insights into Antifolate Resistance

Danny Muzata[1,2#], Dwipanjan Sanyal[3#], Shivram A[1,2], Deeptanshu Pandey[4], Soumyananda Chakraborti[4], Aneesh S. Chivukula[2], Ravi Jasuja[5], Vladimir N. Uversky[6], Daniel Zielinski[7], Prajna D. Upadhyay[2], Mark Albers[8], and Sourav Chowdhury[4*]

Affiliations:

[1] One Health Trust, Bangalore, India

[2] Department of Computer Science and Information Systems, Birla Institute of Technology and Science-Pilani, Hyderabad, India.

[3] Structural Biology and Bioinformatics Division, CSIR-Indian Institute of Chemical Biology, Kolkata, India

[4] Department of Biological Sciences, Birla Institute of Technology and Science-Pilani, Hyderabad, India.

[5] Research Program in Men's Health: Aging and Metabolism, Brigham and Women's Hospital, Harvard Medical School, Boston, Massachusetts, USA

[6] USF Health Byrd Alzheimer's Research Institute, Morsani College of Medicine, University of South Florida, Tampa, FL 33612, USA

[7]Department of Bioengineering, University of California, San Diego, La Jolla, CA, USA

[8]Department of Neurology, Massachusetts General Hospital, Harvard Medical School, Boston, Massachusetts, USA

[*]Corresponding Author:

Sourav Chowdhury
Department of Biological Sciences,
Office: J Block-109,
Birla Institute of Technology and Science, Hyderabad Campus,
Hyderabad, Telangana, India, 500078
Email: sourav.chowdhury@hyderabad.bits-pilani.ac.in

[#]*These authors contributed equally to the work.*

Abstract

The rapid emergence of drug resistance in malaria parasites poses a significant challenge to the efficacy of antifolate treatments. Traditional drug development approaches, which often rely on empirical screening with limited mechanistic insights, tend to overlook the complex evolutionary mechanisms that enable *Plasmodium falciparum* to evade drug inhibition while preserving enzyme functionality. In this study, we employed computational techniques to investigate the mutational landscape of dihydrofolate reductase (DHFR), focusing on regions essential for enzyme stability and resistance. Our analysis uncovered conserved residues essential for stability, mutation hotspots that enhance adaptability under drug pressure and co-evolving clusters revealing critical functional interdependencies. Through integrated approaches including mutational scanning, epistatic interaction modeling, and fitness trajectory mapping, we elucidated distinct evolutionary pathways that drive resistance. We were able to track the adaptive paths taken by wild-type residues upon mutation, revealing the steps required to reach high-fitness peaks within the rugged fitness landscape. These findings provide valuable insights into the molecular mechanisms of antifolate resistance. We suggest that future drug design should target co-evolving networks and conserved regions to support the development of next-generation therapies to overcome resistance.

Keywords: *Malaria***,** *Plasmodium falciparum, Sequence space analysis, Protein fitness, Dihydrofolate reductase, Protein evolution, Antifolate resistance, Folate pathway, Drug design*

Introduction

To date, malaria remains one of the most challenging infectious diseases to control partly due to the parasite's ability to rapidly evolve resistance to frontline drugs[1,2]. Among the most challenging cases of resistance are mutations in *P. falciparum* dihydrofolate reductase (*pf*DHFR), which reduce the effectiveness of antifolate therapies[3,4]. Antifolate drugs have long been used in treating not only malaria but other diseases including bacterial infections and cancer[5,6]. These drugs exert their effects by targeting and inhibiting key enzymes in folate metabolism, a critical pathway for the synthesis of nucleotides and certain amino acids. In *P. falciparum*, several metabolic pathways are targeted by antimalarial drugs. One good example is the hemoglobin degradation pathway and the mitochondrial electron transport chain that is targeted by drugs such as chloroquine and artemisinin[2]. Heat shock proteins also present promising drug targets due to their essential roles in parasite survival and virulence across the various life cycle stages[1]. These alternative drug targets highlight the complexity of *P. falciparum* biology and emphasize the importance of targeting multiple pathways to combat resistance. However, the folate pathway, particularly DHFR, remains one of the most critical targets in antimalarial therapy due to its central role in DNA synthesis and repair[7–9].

In *P. falciparum*, DHFR catalyzes the NADPH-dependent reduction of dihydrofolate to tetrahydrofolate, an essential cofactor required for the synthesis of purines, thymidylate, and certain amino acids[8,10]. This reduction reaction makes DHFR an indispensable enzyme in the folate pathway and a prime target for antifolate drugs such as pyrimethamine and cycloguanil[8,11]. Single and multiple mutations at residue positions 16, 50, 51, 59, 108, and 164 of *pf*DHFR have been linked to antifolate resistance in malaria. Mutations at these sites confer resistance to pyrimethamine and cycloguanil by reducing its binding affinity to the protein rendering the drug less effective[3,12,13].

Despite significant research into DHFR mutations and their role in antifolate resistance, gaps remain in understanding how these mutations affect protein fitness, structure, and function at the molecular level. The concept of sequence space provides a theoretical framework for mapping all possible amino acid combinations in a protein and exploring the evolutionary constraints that shape functional regions. Sequence space analysis has proven valuable in uncovering

evolutionarily constrained regions as well as identifying conserved and flexible sites within protein structures[14]. Thus, in this study, we carried out a thorough sequence space analysis of DHFR protein to explore the evolution of antifolate resistance and its implications for drug design. We developed an evolutionary dynamics simulation model to map adaptive fitness trajectories. This approach integrates both deterministic and stochastic elements, simulating how mutations traverse the fitness landscape while balancing short-term gains and long-term evolutionary potential.

Results

Sequence space analysis

In this study, we explored the sequence space of *pf*DHFR to gain insights into how mutations influence protein fitness and stability. This sequence-based study provided important insights into the protein's evolutionary dynamics. It highlighted how mutations at critical positions influence its stability, function, and mutational tolerance. Through careful analysis of sequence conservation, co-evolution and network-based interactions, we inferred how sequence variability could lead to significant functional consequences in the enzyme, especially in the context of resistance-related mutations.

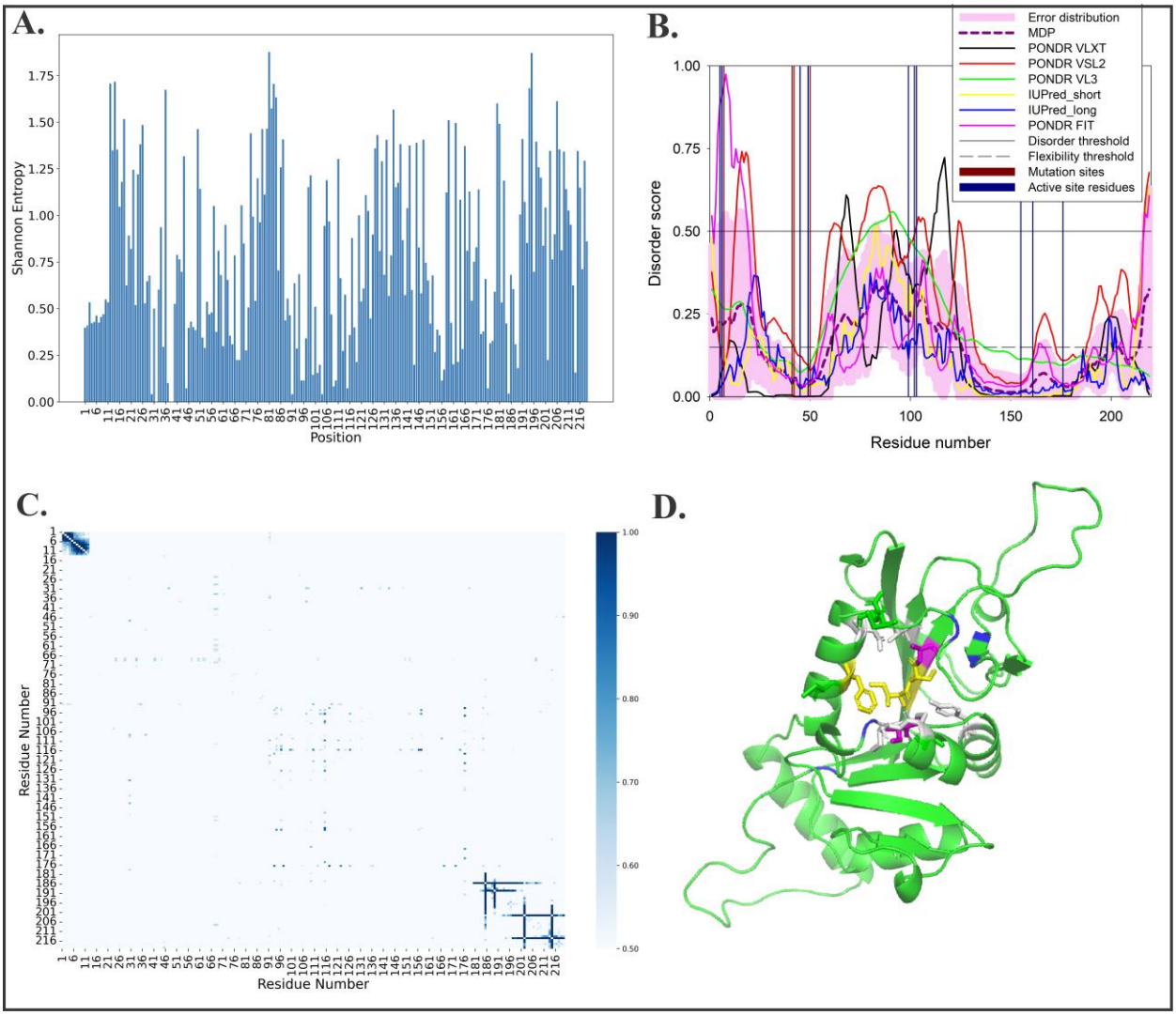

Figure 1: Sequence Space Analysis of DHFR Reveals Key Regions Under Evolutionary Constraints and Functional Adaptation. (A) Shannon Entropy plot shows sequence variability across the DHFR domain. Residues with higher Shannon Entropy scores exhibit greater sequence variability (high spikes), while residues with lower scores (close to zero) are highly conserved. The mutation sites *C41*, *N42*, *C50*, and *S99* exhibit high entropy, indicating their propensity for evolutionary changes. **(B)** Per-residue disorder propensity of pfDHFR evaluated by six commonly used disorder predictors: PONDR® FIT, PONDR® VSL2, PONDR® VL3, PONDR® VLXT, IUPred Short, and IUPred Long. MDP corresponds to the mean disorder profile calculated by averaging the outputs of individual predictors. Residues with disorder scores ≥ 0.5 are considered disordered, while those between 0.15 and 0.5 are flexible. **(C)** The Mutual Information (MI) plot illustrates strong MI values (darker blue) indicating residues that

co-vary. **(D)** 3D structure of the DHFR protein, color-coded by regions of variability and highlighting mutation and active sites. Active site residues are highlighted in yellow sticks, while mutation sites are highlighted in magenta sticks. High-entropy regions in active site are shown in white indicating areas prone to evolutionary change. Highly conserved regions are shown in blue.

Shannon entropy analysis revealed critical positions essential for protein function and mutation-tolerant positions

We performed Shannon Entropy (SE) calculation for each residue position to identify conserved and variable regions within the protein sequence which play a crucial role in the proteins structure and function. Our analysis revealed six conserved residue positions, that is, positions 30, 32, 38, 39, 91 and 104 which exhibited zero entropy values (**Figure 1A**). These regions are likely to be evolutionarily constrained, as mutations in these positions could disrupt protein stability or function. Certain active site positions were also found to be relatively conserved (close to zero) implying that mutations in these positions could have disruptive effects on the pyrimethamine drug binding. Conversely, regions with higher entropy values were identified mostly in the flexible loop regions between residue positions 9–25 and 69–89. Other regions towards the C-terminus (190–219) also displayed high spikes (**Figure 1A**). These positions displayed greater variability, suggesting they may be more tolerant to mutations. Positions C41, N42, C50, and S99 also exhibited high variability and have mutations linked to cycloguanil and pyrimethamine resistance.

Intrinsically disordered prediction revealed that the DHFR is predominantly ordered

We further explored the structural flexibility of the DHFR using six commonly used disorder predictors[15]: PONDR® FIT[16], PONDR® VSL2[17], PONDR® VL3[17], PONDR® VLXT[18], IUPred Short[19], and IUPred Long[19] and generated its disorder profile. The outputs of these predictors were averaged into a mean disorder profile (MDP), providing a consensus view of the protein's disorder propensity. Intrinsic disorder often correlates with regions capable of tolerating mutations contributing to evolutionary flexibility.

Our findings revealed that the DHFR protein is predominantly ordered, with most residues displaying low disorder scores (< 0.5), indicating structural stability. A few flexible regions (disorder scores between 0.15 and 0.5) were identified at positions 1–24, 60–125, 199–203, and 214–219. However, as per the outputs of PONDR® VSL2[17], which is one of the more accurate disorder predictors, several key regions of elevated disorder were identified, that is, residues spanning position 13-21, 61-65, 76-90, 103-107, 123-124, and 217-219. These regions suggest points of potential mutational tolerance, contributing to the protein's adaptability (**Figure 1B**).

Mutual information calculation revealed tight clusters of inter-dependent residues in the N-terminus and C-terminus

While SE calculation offered insights into evolutionary conservation rates, it did not account for interactions between individual residues, particularly how certain positions may evolve in tandem due to structural or functional dependencies. To explore these interactions, we employed Mutual Information (MI) analysis. This measures the co-evolution of residue pairs and identifies compensatory mutations that help maintain protein structure and function. The MI analysis revealed key co-evolutionary relationships between specific residues, providing critical insights into the structural and functional constraints imposed by selective pressures. A high MI value indicates significant positional interdependence, reflecting strong co-evolutionary relationships between residues. In the MI heatmap (**Figure 1C**), dense clusters, such as those seen between residues 1–11 and 181–216, highlight regions with notable co-variation.

MI interaction networks highlight co-evolution of mutational sites in DHFR sequence space

Building on the MI calculations, the graph-based analysis was performed to vividly reveal the complex co-evolutionary relationships between residues in the active site. These MI networks provide a clear visual representation of how different regions of the protein interact. The residue-residue networks provided detailed evidence of epistatic interactions, where mutations at one site could influence compensatory changes at another, preserving enzyme function. The interaction networks for I5 and C6 (**Figure 2A**) demonstrated a tightly knit structural cluster potentially critical for drug-binding and resistance mechanisms. They exhibited strong interactions (MI > 0.8) with residues positions C8, C9, K10, V11, K19, and E12. Residues F49 and I103 also

displayed strong and moderate interactions with M95, I103 and K124, S200, F107, and L110 respectively, suggesting their central role in maintaining the active site configuration.

We extended this analysis to the mutational sites which also revealed intriguing co-evolutionary relationships. Specifically, residues like A7 showed significant interactions with K10, V11 and E12 while C41 interacted strongly with Y61 and K67. Similarly, N42 and C50 formed interactions with Y61 and K67.

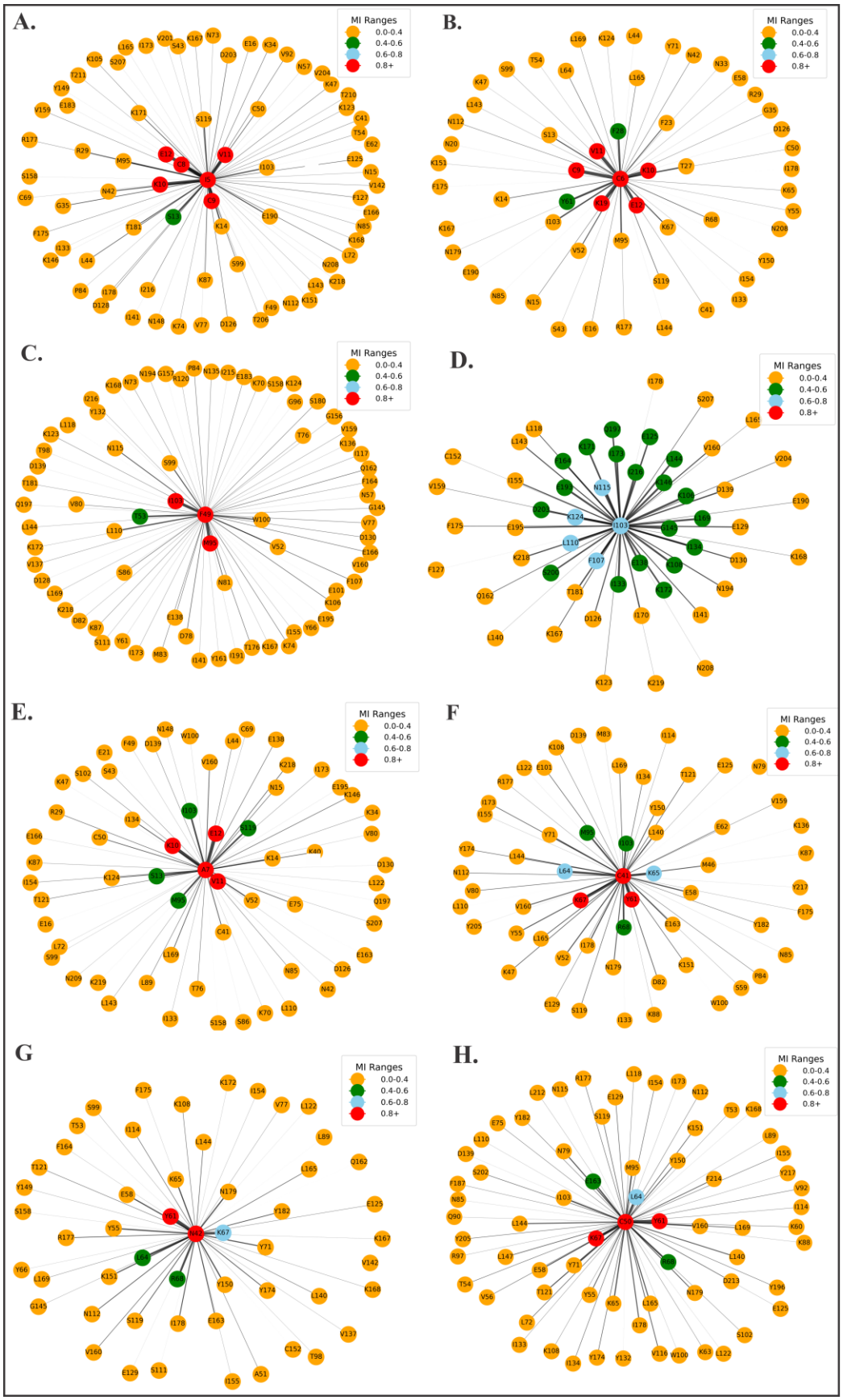
A.
B.
C.
D.
E.
F
G
H.
MI Ranges
0.0-0.4
0.4-0.6
0.6-0.8
0.8+

Figure 2: Mutual Information Networks Reveal Co-evolving Residues Critical for DHFR Function and Adaptation. (**A**) Interaction network for active site **I5**, showing strong MI values with residues like I2, C8, and D1. (**B**) This shows a network centered on active site **C6** with strong interactions extending to K10, V11, and C9, implying that these residues may co-evolve to maintain catalytic function under selective pressures. (**C**) Interaction network for **F49** showing significant interactions with residues such as I103 and T53. (**D**) Interaction network around active site **I103** displayed extensive interactions with several residues such as N115 and K124 highlighting the interconnectedness of residues involved in DHFR's active site dynamics. (**E**) Interaction network centered on mutation site **A7** showing significant correlations with residues such as V11, A4, and K10. (**F**) Network around mutation site C41, displaying strong MI interactions with residues like K55 and C9. (**G**) Mutation site N42 shows strong interactions with W103 and K67 (**H**) Network focused on mutation site C50 highlights strong interactions with residues K55 and V11.

Maximal clique analysis and community detection identified densely connected cliques

In our study, we performed Maximal Clique Analysis (MCA)[20,21] and Community Detection[22] to identify densely connected sub-networks (cliques) and partition the protein into distinct interaction groups. These analyses provide a deeper layer of insight compared to MI analysis, as they go beyond pairwise interactions by revealing how clusters of residues interact within a broader network. Important cliques were identified in regions containing known active and mutation sites, including residues 6, 7, 42, 49, 155 (**Figure 3A**). These residues form part of highly interconnected clusters, indicating strong structural and functional interdependencies.

Residues 49 and 155, which form part of pyrimethamine-binding pocket, were observed in multiple cliques alongside other critical residues highlighting their importance in stabilizing the surrounding structural framework of the protein. Mutation sites such as residues 7 and 42 also formed part of distinct cliques where they interacted with other residues. It is worth noting that residue 6, a drug-binding pocket, was identified within the same clique as residue 7, a known mutation site. The analysis revealed that the active sites and mutation sites often reside in highly interconnected cliques, suggesting that mutations at these sites might affect the stability and function of nearby residues through their cooperative interactions. Community detection (**Figure**

3B) further uncovered broader groupings of residues that frequently interact within the same sub-network. It highlighted functional domains or regions that evolve together.

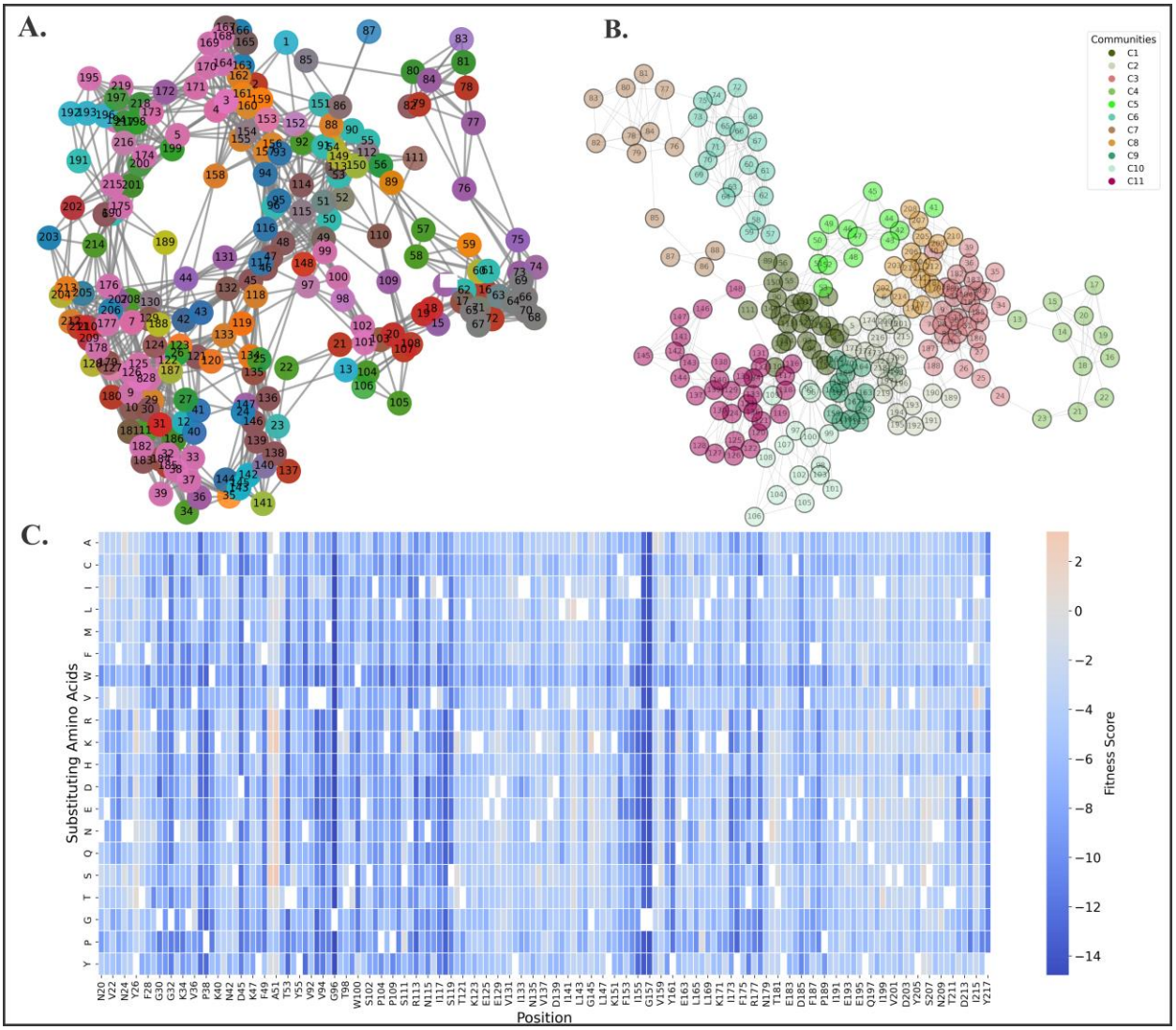

Figure 3: **Maximal Clique and Mutational Sensitivity Analyses Reveal Inter-Residue Networks and Evolutionarily Constrained Regions in DHFR.** (**A**) Maximal clique detection analysis visualizes cliques or complete subgraphs within the DHFR residue network. Different cliques represent tightly connected regions of residues which indicate areas of high inter-residue coordination and co-evolution. (**B**) Community detection analysis using a modularity-based algorithm identified 11 distinct communities within the DHFR protein. These communities represent clusters of residues that are likely to have high intra-group connectivity. (**C**) Deep mutational scan heatmap showing the fitness effects of single amino acid substitutions across the

DHFR protein. The heatmap reveals positions that are highly sensitive to mutations, with dark blue indicating deleterious effects (negative fitness scores) and light shades or orange representing beneficial or neutral mutations.

Deep mutational scanning yielded mutational hotspots with beneficial fitness effects that may facilitate evolutionary adaptation under drug pressure.

The Deep Mutational Scanning (DMS) analysis was performed to gain insights into the functional consequences of amino acid substitutions across the protein sequence. By quantifying the fitness effects of each mutation, this analysis allowed us to map the sequence space of DHFR, identifying regions that are intolerant to mutations, as well as those that can tolerate or even benefit from substitutions. A significant number of deleterious mutations were observed in key regions of the DHFR enzyme (**Figure 3C**), particularly around the active site. Positions such as I155, which is a critical residue within the active site, show dramatic reductions in fitness for nearly all substitutions. This suggests that I155 plays an essential role in maintaining the enzyme's catalytic function and structural stability. Similarly, D45, F49 and I155, another set of residues located in the active site, also shows a strong deleterious signal upon mutation with almost all substitutions. The positions G96, G156, G157 and Y217 strongly emerged as key sites where mutations lead to significant fitness losses. These residues are situated near the catalytic core of the enzyme and substitutions here likely disrupt the enzyme's stability or interfere with essential catalytic processes. The DMS analysis also uncovered key mutation hotspots with beneficial fitness effects, particularly in the regions spanning residues 120 to 155 and 190 to 211.

The fitness trajectories for active site residues illustrates distinct adaptive paths for various mutations, highlighting the complexity of the fitness landscape for pfDHFR

Our fitness trajectory analysis provides critical insights into the distinct adaptive pathways of key active site residues in *pf*DHFR. This reveals how the enzyme navigates complex fitness landscapes under selective pressure. To simulate these evolutionary paths, we developed an epistasis-based fitness prediction model using Dijkstra’s shortest path algorithm. In this model, mutations are represented as nodes, and the edges between them are weighted by the absolute fitness differences between the mutations. This approach identifies the most efficient mutational

paths—those requiring the fewest steps—from the wild-type to both local and global fitness peaks. The model captures both stochastic and deterministic evolutionary dynamics, offering a realistic framework for simulating biological evolution. Stochastic sampling introduces randomness, reflecting genetic drift and the exploration of multiple paths. Deterministically, the algorithm favors mutations with immediate fitness benefits, emulating natural selection. This dual approach balances short-term incremental adaptation with long-distance evolutionary leaps**,** mirroring the unpredictable yet selective nature of real-world evolution.

Using deep mutational scan data to guide these pathways, the model reveals how near-neutral and compensatory mutations expand the genotype-phenotype space. This allows the enzyme to smooth rugged fitness landscapes and adapt under selective pressure. For instance, mutations at position 49 exhibited quick transitions to fitness peaks such as A51S, highlighting the mutational tolerance at this site. However, other substitutions at the same site, such as F49K and F49W, required longer pathways to reach comparable peaks, indicating variability in their fitness effects (**Figure 4A**). Similarly, mutations S99C and S99T demonstrated shorter evolutionary paths to local fitness peaks like C50S, suggesting faster adaptation, while mutations like S99F followed more extended trajectories (**Figure 4C**). This trend was also observed at positions 102 and 103, with certain mutations achieving rapid adaptation, while others required more gradual, complex walks. Conversely, position 155 presented one of the most challenging landscapes, with most mutations demanding over 100 evolutionary steps to achieve fitness peaks (**Figure 4F**). A comparable trend was seen at position 161 (**Figure 4H**), where mutations such as Y161L and Y161K required long evolutionary walks toward global peaks, highlighting the ruggedness of the landscape at these critical sites.

These findings underscore that evolutionary adaptation in DHFR is not uniform. While certain residues, such as 49 and 99, serve as stepping stones toward resistance by facilitating quick fitness gains, others like 155 demand more extensive evolutionary navigation. The interplay between stochastic exploration and deterministic selection captured by our model reflects the intricate dynamics of DHFR evolution, offering a deeper understanding of how the enzyme balances adaptability and functional constraints under selective pressure.

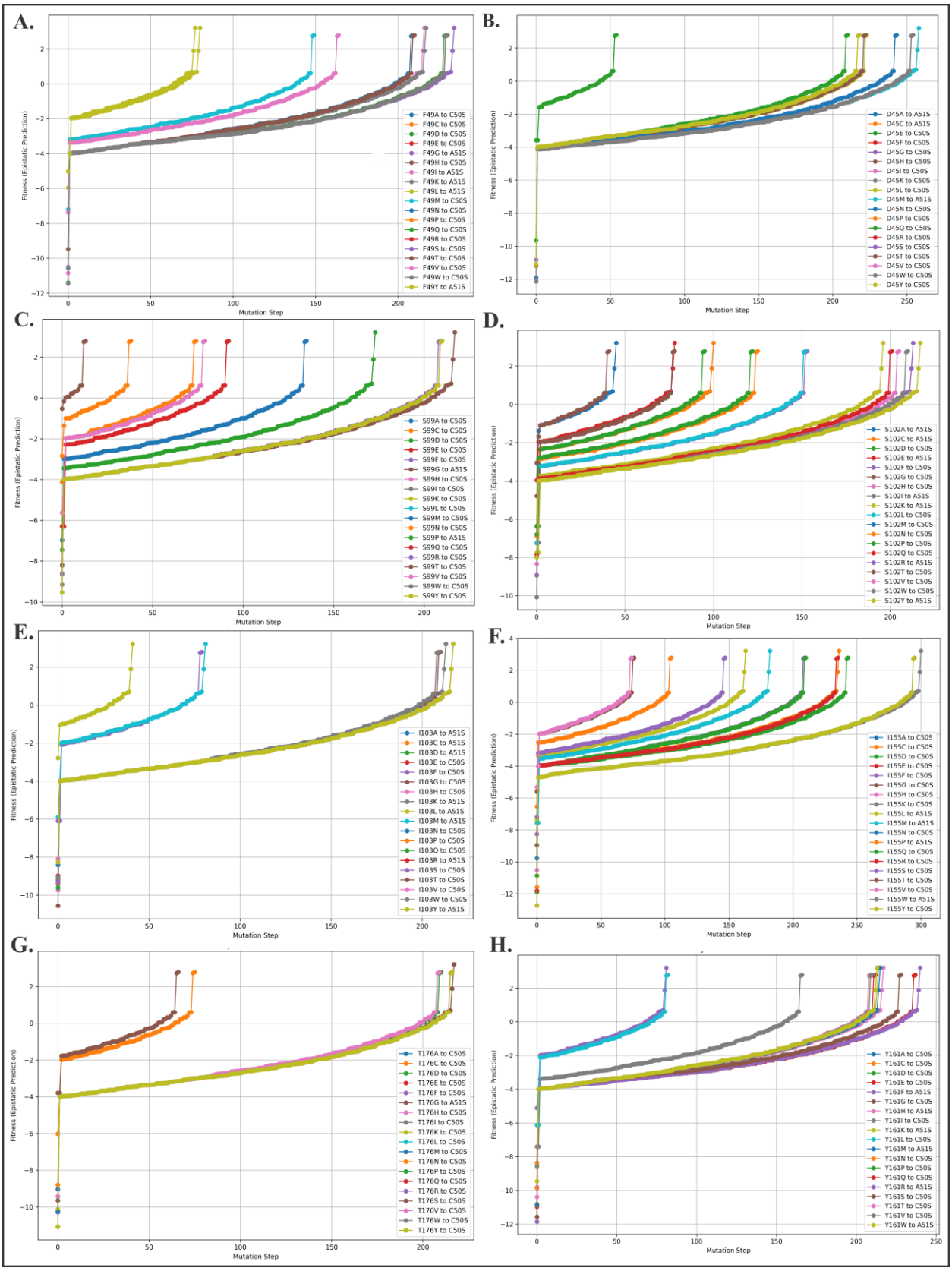
A.
Fitness (Epistatic Prediction)
Mutation Step
F49A to C50S
F49C to C50S
F49D to C50S
F49E to C50S
F49G to A51S
F49H to C50S
F49I to A51S
F49K to A51S
F49L to A51S
F49M to C50S
F49N to C50S
F49P to C50S
F49Q to C50S
F49R to C50S
F49S to C50S
F49T to C50S
F49V to C50S
F49W to C50S
F49Y to A51S
B.
Fitness (Epistatic Prediction)
Mutation Step
D45A to A51S
D45C to A51S
D45E to C50S
D45F to C50S
D45G to C50S
D45H to C50S
D45I to C50S
D45K to C50S
D45L to C50S
D45M to A51S
D45N to C50S
D45P to C50S
D45Q to C50S
D45R to C50S
D45S to C50S
D45T to C50S
D45V to C50S
D45W to C50S
D45Y to C50S
C.
Fitness (Epistatic Prediction)
Mutation Step
S99A to C50S
S99C to C50S
S99D to C50S
S99E to C50S
S99F to C50S
S99G to A51S
S99H to C50S
S99I to C50S
S99K to C50S
S99L to C50S
S99M to C50S
S99N to C50S
S99P to A51S
S99Q to C50S
S99R to C50S
S99T to C50S
S99V to C50S
S99W to C50S
S99Y to C50S
D.
Fitness (Epistatic Prediction)
Mutation Step
S102A to A51S
S102C to A51S
S102D to C50S
S102E to A51S
S102F to C50S
S102G to C50S
S102H to C50S
S102I to A51S
S102K to A51S
S102L to C50S
S102M to C50S
S102N to C50S
S102P to C50S
S102Q to C50S
S102R to A51S
S102T to C50S
S102V to C50S
S102W to C50S
S102Y to A51S
E.
Fitness (Epistatic Prediction)
Mutation Step
I103A to A51S
I103C to A51S
I103D to A51S
I103E to C50S
I103F to C50S
I103G to C50S
I103H to C50S
I103K to A51S
I103L to A51S
I103M to A51S
I103N to C50S
I103P to C50S
I103Q to C50S
I103R to A51S
I103S to C50S
I103T to C50S
I103V to C50S
I103W to C50S
I103Y to A51S
F.
Fitness (Epistatic Prediction)
Mutation Step
I155A to C50S
I155C to C50S
I155D to C50S
I155E to C50S
I155F to C50S
I155G to C50S
I155H to C50S
I155K to C50S
I155L to A51S
I155M to A51S
I155N to C50S
I155P to A51S
I155Q to C50S
I155R to C50S
I155S to C50S
I155T to C50S
I155V to C50S
I155W to A51S
I155Y to C50S
G.
Fitness (Epistatic Prediction)
Mutation Step
T176A to C50S
T176C to C50S
T176D to C50S
T176E to C50S
T176F to C50S
T176G to A51S
T176H to C50S
T176I to C50S
T176K to C50S
T176L to C50S
T176M to C50S
T176N to C50S
T176P to C50S
T176Q to C50S
T176R to C50S
T176S to C50S
T176V to C50S
T176W to C50S
T176Y to C50S
H.
Fitness (Epistatic Prediction)
Mutation Step
Y161A to C50S
Y161C to C50S
Y161D to C50S
Y161E to C50S
Y161F to A51S
Y161G to C50S
Y161H to A51S
Y161I to C50S
Y161K to A51S
Y161L to C50S
Y161M to A51S
Y161N to C50S
Y161P to C50S
Y161Q to C50S
Y161R to A51S
Y161S to C50S
Y161T to C50S
Y161V to C50S
Y161W to A51S

281

Figure 4: **Fitness Trajectories Highlight Adaptive Paths of Key Active Site Residues in DHFR. (A)** At position 49, mutations such as F49L and F49Y achieve quicker routes to fitness peaks, while others like F49K, F49W, and F49H follow longer, more gradual trajectories. **(B)** Position 45 shows gradual fitness increases across all mutations, except D45E which achieved a relatively quicker fitness. **(C)** Mutations at position 99 exhibit variability in trajectory length. Positions S99T and S99C reach fitness peaks faster, while S99G requires the longest path. **(D)** Position 102 shows variation in mutation paths, with S102A and S102P achieving fitness improvements more quickly than S102E and S102F. **(E)** Mutations at positions 103 generally follow longer trajectories to fitness peaks. **(F)** At position 155, most mutations require extended walks of over 100 steps to reach fitness peaks. **(G)** Shows similar patterns at position 161, where Y161L and Y161K mutations follow longer trajectories. **(H)** Position 176 demonstrates both short and long trajectories, with some mutations reaching fitness peaks more rapidly, while others require extended adaptive steps.

Discussion

The folate pathway plays a crucial role in the survival of *P. falciparum* by supplying essential cofactors for nucleotide and amino acid synthesis[7]. This makes DHFR a prime target for antifolate drugs. However, the emergence of resistance mutations in this essential protein has led to significant challenges in the effective treatment of malaria. These mutations have enabled the parasite to evade drug inhibition while preserving enzyme functionality[23]. Further complexity arises from the genomic organization of the *pfdhfr-ts* gene. This is a bifunctional gene located on chromosome 4 that encodes both DHFR and thymidylate synthase within the same polypeptide chain[24,25]. This dual functionality introduces potential pleiotropic effects, where mutations selected for resistance in the DHFR domain could unintentionally affect the function of the TS domain, or vice versa. Similar to the observations of Raff and Kaufman[26], such interdependencies highlight the complexity of interconnected biological systems, where targeted changes can yield large-scale, unintended consequences across multiple functions. The interdependence between these two enzymatic activities creates challenges in predicting the evolutionary consequences of mutations, as adaptations beneficial for one activity might impair

the other. While the direct impact of promoter mutations on this gene remains largely unexplored[27], these mutations could potentially influence gene dosage and expression levels, thereby affecting drug resistance mechanisms. This genomic context implies that resistance arises not only from individual enzyme mutations but also from the complex regulation of gene expression. Thus, understanding the evolutionary dynamics driving these mutational escapes in DHFR is essential for designing novel antifolate therapies.

Mutational landscapes are inherently complex[28], reflecting the diverse roles amino acid substitutions play in shaping protein function and evolution. Proteins, including DHFR, are subjected to a range of evolutionary pressures that necessitate both structural stability and adaptability[29,30]. However, mutations that confer drug resistance often introduce trade-offs that impact their fitness[31]. This balance is complicated by the fact that near-neutral mutations, while individually minor, can act as stepping stones toward significant adaptive shifts[32]. The study of mutational landscapes using tools such as deep mutational scanning has proven critical in identifying mutations that influence protein adaptability without drastic functional compromises[33,34]. Some mutations improve fitness only marginally but, over time, accumulate to confer drug resistance[35]. These insights highlight how proteins like DHFR navigate a rugged landscape, with regions of both mutational tolerance and structural constraint. This understanding is essential for predicting the evolution of resistance and identifying critical points for therapeutic intervention.

The evolutionary landscape of proteins is defined by peaks of high fitness separated by valleys of low fitness. This ruggedness reflects the complex interplay between mutations, structural integrity, and functional performance. Adaptive walks along this landscape often involve both stochastic exploration and deterministic processes that select for advantageous traits[36]. Near-neutral mutations facilitate exploration by expanding the search space which allows enzymes to navigate fitness valleys more efficiently[32]. Over time, these mutations can accumulate to provide a selective advantage, especially under environmental pressures. Evolutionary trajectories are further shaped by epistasis, where interactions between multiple mutations influence fitness outcomes[37]. These complexities emphasize the importance of studying not just individual mutations but also their collective impact on protein function.

The present study provides critical insights into the mutational and evolutionary landscapes of *P. falciparum* DHFR with emphasis on both structural constraints and adaptive strategies employed by the protein. Conserved residues were identified and highlighted as structurally indispensable elements that are less tolerant to mutations. These regions offer promising targets for novel antifolate therapies, as disrupting them could impair the parasite's ability to maintain functionality and evolve resistance. Network-based analyses further revealed key hubs and cliques of interacting residues. The presence of such interconnected, co-evolving clusters highlights that resistance arises not through isolated mutations but via cooperative networks that preserve stability despite structural alterations. Several mutation hotspots were also identified with beneficial fitness effects, particularly in regions spanning residues 120–155 and 190–211. While many mutations, especially at key active site residues like I155, D45, and F49, caused significant fitness losses due to their critical role in protein stability, certain regions exhibited greater tolerance to substitutions. These mutation-tolerant regions suggest potential adaptive flexibility which enable the enzyme to navigate selective pressures by accommodating beneficial changes without compromising overall functionality. The integration of conserved elements, mutation hotspots, co-evolving clusters, and interconnected networks underscores the multifaceted nature of resistance. Targeting these networks and conserved regions provides a promising approach for the development of future-proof antifolate therapies, disrupting the parasite’s ability to adapt and evolve in response to drug pressure.

To simulate adaptive evolutionary pathways and explore how mutations influence fitness landscapes, we developed an epistatic fitness prediction model. Our model provides valuable insights into how *P. falciparum* DHFR navigates complex fitness landscapes under selective pressure. This dual framework captures the unpredictable aspects of evolution while also reflecting selective pressures that favor beneficial mutations. Through this approach, we modeled both rapid adaptive walks and gradual evolutionary trajectories, mirroring the diverse paths proteins take toward higher fitness in dynamic environments. The use of deep mutational scan data enabled us to assign fitness values to individual mutations. This provided a quantitative lens to evaluate how various mutations affect enzyme stability and function. By mapping these trajectories, we demonstrated that near-neutral mutations and compensatory interactions play pivotal roles in expanding the genotype-phenotype space, thereby smoothing the rugged fitness

landscape. This adaptive flexibility allows DHFR to navigate resistance pathways efficiently, overcoming mutational barriers while retaining functionality.

The insights from this model emphasize the importance of epistatic interactions—where mutations at one site influence the fitness outcomes of others—in shaping evolutionary pathways. It underscores that resistance in DHFR is not merely a product of isolated mutations but rather emerges from complex mutational networks that facilitate both short-term gains and long-term adaptability. This predictive framework enhances our understanding of antifolate resistance mechanisms and lays the groundwork for designing novel antifolate therapies that can effectively disrupt these evolutionary strategies.

While our study offers significant insights into the evolution of antifolate resistance, it is not without limitations. This research was solely based on protein sequence analysis and did not delve into the structural dynamics of DHFR, which could provide additional insights into enzyme stability, conformational changes, and protein-drug interactions. Despite incorporating stochastic sampling to simulate randomness in evolutionary choices, the model may still miss certain complexities of real-world adaptation, such as temporary fitness losses or parallel exploration of multiple paths. These limitations highlight the challenges of representing rugged fitness landscapes, where local optima may be revisited and evolutionary trajectories can follow non-linear patterns over time. Moreover, the limited availability of fitness data constrains the scope of the fitness landscape explored. Expanding the dataset or integrating complementary experimental data would provide a more comprehensive view of mutational effects across a broader range of residues. Future experimental validation of our computational findings is crucial. Molecular docking simulations and fitness assays in biological systems will confirm whether the identified adaptive pathways correspond to real-world resistance mechanisms. Integrating advanced computational tools, such as machine learning models, could enhance predictive accuracy and uncover novel mutational pathways that are difficult to identify using conventional algorithms. These efforts will contribute to the development of future-proof antifolate therapies capable of addressing the challenges posed by evolving resistance in *P. falciparum*.

Materials and Methods

Sequences preprocessing

For this study, we used the crystal structure of the wild-type *P. falciparum* DHFR-TS protein (PDB ID: 3QGT) as the reference for our analyses. The protein structure consists of two domains: the DHFR domain (first 231 residues) and the TS domain (last 288 residues), separated by an 89-residue interjunction region (Supplemental Figure 1). Given the focus on DHFR, we truncated the DHFR domain, which stretches from amino acid position 10 to 228 in the full-length protein as annotated in UNIPROT[38]. This truncation was performed using the PYMOL Molecular Graphics System (version 3.0.3)[39]. For consistency, the truncated sequence was re-indexed from 1 to 219, a scheme used throughout the study.

Homology Modeling and Structure Validation

Upon examination, the DHFR protein contained ten missing residues in its sequence from position 86 to 95. To fill in these gaps, homology modeling was performed using Modeller (Version 10.5)[40,41]. This software generated several structural models and ranked them using the Discrete Optimized Protein Energy (DOPE) scoring function. The model with the lowest DOPE score was selected as the most accurate representation of the full DHFR structure (**Supplemental Figure 2**). To ensure the accuracy of the modeled structure, we calculated the Root Mean Square Deviation (RMSD) between the modeled residues and the crystal structure (**Supplemental Figure 3**). An RMSD value of 0.306 Å indicated high structural similarity. After validation, we extracted the amino acid sequence (219 residues) from the modeled DHFR structure for further analyses.

Sequence Space Analysis

To explore the mutational landscape of DHFR, we performed a sequence space analysis using the multiple sequence alignment (MSA) of homologous DHFR proteins. First, we retrieved 5000 non-redundant protein sequences homologous to DHFR using the NCBI BlastP tool[42]. The sequences were cleaned to ensure high quality, non-redundancy and biological relevance. We then aligned the cleaned sequences using the ClustalW algorithm[43], and the resulting MSA served as the basis for the subsequent analyses.

Occupancy Calculation

Occupancy calculations were performed to assess how frequently specific amino acids occupy each residue position in homologous DHFR sequences. Positions with high occupancy values represent conserved residues, likely essential for the protein's structural stability. By comparing occupancy data with mutation sites, we identified residues where mutations may have significant impacts on the protein's structure and function.

Shannon Entropy Calculation

Shannon entropy (S(*i*))[44] was calculated to quantify the variability of amino acids at each sequence position. Positions with low entropy values represent conserved residues, critical for structural and functional integrity, while high entropy values indicate positions prone to mutations.

$$S(i) = -\sum_{a_i=1}^{20} P(a_i)\, logP(a_i)$$

Where ***i*** represents the sequence position, and ***P(a_i)*** is the probability of amino acid ***a*** occurring at position ***i*** in the MSA. Lower values of ***S(i)*** correspond to highly conserved residues, while higher values suggest increased variability.

Mutual Information Calculation

To investigate co-evolving residues, we calculated mutual information (MI)[45,46] for each pair of positions in the MSA. MI quantifies the degree of correlation between two sequence positions, revealing residues that might be functionally or structurally interdependent. These co-varying residues could indicate regions where mutational compensation occurs, maintaining overall protein function despite mutations in specific positions.

$$MI(i, j) = \sum_{a_i=1}^{21} \sum_{b_j=1}^{21} P(a_i, b_j) \log \frac{P(a_i, b_j)}{P(a_i)\, P(b_j)}$$

In this formula, $P(ai, bj)$ represents the probability of amino acids a and b occurring at positions *i* and *j*, respectively, while $P(a_i)$ and $P(b_j)$ are the individual probabilities at each position . The $MI(i,j)$ values range from 0 (uncorrelated residues) to MI_{max} (the most interdependent residue pairs). In this study, a cutoff MI value of 0.5 was chosen to focus on highly co-varying positions. The MI values were visualized as a heatmap and a co-evolutionary matrix, generated using python programming.

Intrinsic Disorder Prediction

Intrinsic disorder prediction analysis was conducted to explore the presence of disordered regions within the DHFR protein. Disordered regions, known for their inherent flexibility, can tolerate higher levels of mutation and often play significant roles in protein-protein interactions. For a comprehensive evaluation, we employed six widely used disorder predictors: PONDR® FIT[16], PONDR® VSL2[17], PONDR® VL3[17], PONDR® VLXT[18], IUPred Short[19], and IUPred Long[19]. These predictors leverage distinct predictive approaches to identify disordered regions within the protein. PONDR® VSL2 is particularly optimized for proteins containing both structured and disordered regions[47]. By integrating the outputs from all six predictors, we generated a mean disorder profile (MDP), providing a consensus disorder score for each residue. Residues with scores above 0.5 were classified as disordered, while those between 0.15 and 0.5 were considered flexible but ordered. This disorder profile was further analyzed to examine potential correlations between disordered regions, known mutation sites, and active site residues, helping to elucidate the role of structural flexibility in resistance mutations and the maintenance of protein function.

Graph-Based Analysis

Following the MI calculations, we performed a graph-based analysis of the identified co-evolving residues. Nodes in the graph represent individual residues, while edges denote strong mutual information-based connections between them. The MI threshold was used to define the strength of these interactions, with different ranges highlighting strong ($MI > 0.8$), moderate ($0.6 < MI < 0.8$), and weak ($0.4 < MI < 0.6$) interactions. This graph-based analysis allowed us to visualize key mutation sites (A16, N42, C50, S99, S108, and I155) and their network of

interactions, especially with active site residues. The resulting network graphs provided insight into how mutations at specific residues might influence structural stability and drug resistance through interdependencies with nearby residues.

To investigate densely connected sub-networks within the DHFR protein, we employed Maximal Clique Analysis (MCA)[20,21] and Community Detection[22] methods. In MCA, we aimed to identify groups of residues that form maximal cliques, where every residue (node) within a clique is directly connected to every other residue. This method focuses on identifying highly interconnected sets of residues that are structurally and functionally interdependent. Each residue in the protein is represented as a node and the edges between these nodes represent significant interactions, which are based on proximity in the protein structure or known co-evolutionary relationships. The primary goal was to identify the largest cliques within the overall interaction network. Community detection was also performed to divide the protein's residue interaction network into distinct subgroups or communities. Unlike MCA, which focuses on fully connected sub-networks, community detection identifies groups of residues that are more likely to interact within their community than with residues outside it.

Fitness Trajectories Analysis Using Epistatic Prediction Model

To explore the epistatic interactions between multiple mutations, we developed an epistasis-based fitness prediction model to simulate adaptive walks within the *P. falciparum* DHFR protein. The model integrates both stochastic and deterministic elements to account for the complexity of the fitness landscape. The epistatic data used were derived from deep mutation scan which predict the fitness effects of individual mutations. The goal of this analysis was to map the evolutionary trajectories of key active site residues as they navigate through the fitness landscape.

We used Dijkstra's shortest path algorithm[48] to construct the adaptive walks, representing the protein's potential mutational paths in search of fitness improvement. In this graph-based approach, mutations were treated as nodes, and fitness differences between mutations as weighted edges. The shortest path corresponds to the fewest evolutionary steps required to maximize fitness. The fitness values for each mutation were calculated from the epistatic

prediction data, where a positive value indicates a beneficial mutation and a negative value represents a deleterious one. Given that a set of mutations $M = \{m_1, m_2, \ldots, m_n\}$ and their fitness values $f(m_i)$, our goal was to identify the shortest adaptive walk that maximizes fitness. The distance between two mutations is defined as the absolute difference between their fitness values;

$$d(m_i, m_j) = | f(m_i) - f(m_j) |$$

We sought to find the mutation path P from an initial wild-type m_{wt} to a final high-fitness peak mutation m_{peak}, such that the sum of fitness differences along the path is minimized;

$$P = \arg min \sum_{i=1}^{k-1} d(m_i, m_{i+1})$$

A combination of deterministic and stochastic methods was employed. The algorithm deterministically follows the mutation path with the highest fitness improvement, i.e., aiming directly for the global peak unless the local peak provides a substantially higher immediate fitness gain. When multiple peaks are available, the algorithm stochastically samples between the local and global peaks based on fitness differences. The stochastic component is controlled by a probability threshold, which adjusts based on the fitness difference between the local peak and the global peak:

$$\text{probability threshold} = \begin{cases} 0.3 & \text{if } \Delta f > 2 \\ 0.5 & \text{if } 1 < \Delta f \leq 2 \\ 0.7 & \text{if } \Delta f \leq 1 \end{cases}$$

This threshold governs the likelihood of choosing a local versus a global peak, simulating a situation where evolutionary pressures might favor local exploration or long-distance leaps to distant fitness peaks.

AUTHOR CONTRIBUTIONS

SC and DS conceived and planned the work. SC motivated and guided the work. DM performed all the formal analysis, model development, manuscript composition, and critical review. VNU performed the disorder analysis. SC, DS, VNU, SA, ASC, DZ, RJ and PDU provided critical feedback and assisted in refining the manuscript.

ACKNOWLEDGMENT

DM acknowledges One Health Trust, Bangalore, India. DM and SC acknowledge the Director, Birla Institute of Technology and Science-Pilani, Hyderabad, India.

DECLARATION

The authors declare that they have no conflicts of interest.

DATA AVAILABILITY STATEMENT

The data that support the findings of this study are available from the corresponding author upon reasonable request.

References

1. Ahmad T, Alhammadi BA, Almaazmi SY, Arafa S, Blatch GL, Dutta T, et al. Plasmodium falciparum heat shock proteins as antimalarial drug targets: An update. Cell Stress and Chaperones. 2024 Apr 1;29(2):326–37.

2. Huthmacher C, Hoppe A, Bulik S, Holzhütter HG. Antimalarial drug targets in Plasmodium falciparum predicted by stage-specific metabolic network analysis. BMC Systems Biology. 2010 Aug 31;4(1):120.

3. Sirawaraporn W, Prapunwattana P, Sirawaraporn R, Yuthavong Y, Santi DV. The dihydrofolate reductase domain of Plasmodium falciparum thymidylate synthase-dihydrofolate reductase. Gene synthesis, expression, and anti-folate-resistant mutants. Journal of Biological Chemistry. 1993 Oct 15;268(29):21637–44.

4. Kreutzfeld O, Tumwebaze PK, Byaruhanga O, Katairo T, Okitwi M, Orena S, et al. Decreased Susceptibility to Dihydrofolate Reductase Inhibitors Associated With Genetic Polymorphisms in Ugandan Plasmodium falciparum Isolates. J Infect Dis. 2021 Aug 30;225(4):696–704.

5. Wróbel A, Arciszewska K, Maliszewski D, Drozdowska D. Trimethoprim and other nonclassical antifolates an excellent template for searching modifications of dihydrofolate reductase enzyme inhibitors. J Antibiot. 2020 Jan;73(1):5–27.

6. Fernández-Villa D, Aguilar MR, Rojo L. Folic Acid Antagonists: Antimicrobial and Immunomodulating Mechanisms and Applications. Int J Mol Sci. 2019 Oct 9;20(20):4996.

7. Hyde JE. Exploring the folate pathway in Plasmodium falciparum. Acta Trop. 2005 Jun;94(3):191–206.

8. Bilsland E, Van Vliet L, Williams K, Feltham J, Carrasco MP, Fotoran WL, et al. Plasmodium dihydrofolate reductase is a second enzyme target for the antimalarial action of triclosan. Sci Rep. 2018 Jan 18;8(1):1038.

9. Nzila A, Ward SA, Marsh K, Sims PF, Hyde JE. Comparative folate metabolism in humans and malaria parasites (part I): pointers for malaria treatment from cancer chemotherapy. Trends in parasitology. 2005 Jun;21(6):292.

10. Chusacultanachai S, Thiensathit P, Tarnchompoo B, Sirawaraporn W, Yuthavong Y. Novel antifolate resistant mutations of *Plasmodium falciparum* dihydrofolate reductase selected in *Escherichia coli*. Molecular and Biochemical Parasitology. 2002 Mar 1;120(1):61–72.

11. Yuthavong Y, Tarnchompoo B, Vilaivan T, Chitnumsub P, Kamchonwongpaisan S, Charman SA, et al. Malarial dihydrofolate reductase as a paradigm for drug development against a resistance-compromised target. Proc Natl Acad Sci U S A. 2012 Oct 16;109(42):16823–8.

12. Kayode AT, Ajogbasile FV, Akano K, Uwanibe JN, Oluniyi PE, Eromon PJ, et al. Polymorphisms in Plasmodium falciparum dihydropteroate synthetase and dihydrofolate reductase genes in Nigerian children with uncomplicated malaria using high-resolution melting technique. Sci Rep. 2021 Jan 12;11(1):1–8.

13. Amusengeri A, Tata RB, Tastan Bishop Ö. Understanding the Pyrimethamine Drug Resistance Mechanism via Combined Molecular Dynamics and Dynamic Residue Network Analysis. Molecules. 2020 Feb 18;25(4):904.

14. Sanyal D, Banerjee S, Bej A, Chowdhury VR, Uversky VN, Chowdhury S, et al. An integrated understanding of the evolutionary and structural features of the SARS-CoV-2 spike receptor binding domain (RBD). International Journal of Biological Macromolecules. 2022 Sep;217:492–505.

15. Dayhoff II GW, Uversky VN. Rapid prediction and analysis of protein intrinsic disorder. Protein Science. 2022;31(12):e4496.

16. Xue B, Dunbrack RL, Williams RW, Dunker AK, Uversky VN. PONDR-FIT: A Meta-Predictor of Intrinsically Disordered Amino Acids. Biochimica et biophysica acta. 2010 Jan 25;1804(4):996.

17. Peng K, Radivojac P, Vucetic S, Dunker AK, Obradovic Z. Length-dependent prediction of protein intrinsic disorder. BMC Bioinformatics. 2006 Apr 17;7(1):208.

18. Romero P, Obradovic Z, Li X, Garner EC, Brown CJ, Dunker AK. Sequence complexity of disordered protein. Proteins. 2001 Jan 1;42(1):38–48.

19. Dosztányi Z, Csizmók V, Tompa P, Simon I. The pairwise energy content estimated from amino acid composition discriminates between folded and intrinsically unstructured proteins. J Mol Biol. 2005 Apr 8;347(4):827–39.

20. Pardalos PM, Rodgers GP. A branch and bound algorithm for the maximum clique problem. Computers & Operations Research. 1992 Jul 1;19(5):363–75.

21. Konc J, Janezic D. An improved branch and bound algorithm for the maximum clique problem. MATCH Commun Math Comput Chem. 2007;58, 569-590.

22. Grant WP, Ahnert SE. Modular decomposition of protein structure using community detection. Journal of Complex Networks. 2019 Feb 1;7(1):101–13.

23. Heinberg A, Kirkman L. The molecular basis of antifolate resistance in Plasmodium falciparum: looking beyond point mutations. Ann N Y Acad Sci. 2015 Apr;1342(1):10–8.

24. Dj B, Wb L, T H, J I. Molecular cloning and sequence analysis of the Plasmodium falciparum dihydrofolate reductase-thymidylate synthase gene. Proceedings of the National Academy of Sciences of the United States of America [Internet]. 1987 Dec [cited 2024 Oct 7];84(23). Available from: https://pubmed.ncbi.nlm.nih.gov/2825189/

25. Mita T, Tanabe K, Kita K. Spread and evolution of Plasmodium falciparum drug resistance. Parasitology International. 2009 Sep;58(3):201–9.

26. Garfield DA, Wray GA. The Evolution of Gene Regulatory Interactions. BioScience. 2010 Jan 1;60(1):15–23.

27. Ferreira de Azevedo M, del Portillo HA. Control of Gene Expression in Plasmodium. 2006 Jul 17 [Updated 2007 May 11]. In: Gruber A, Durham AM, Huynh C, et al., editors. Bioinformatics in Tropical Disease Research: A Practical and Case-Study Approach [Internet]. Bethesda (MD): National Center for Biotechnology Information (US); 2008. Chapter B01.

28. Wagner A. Evolvability-enhancing mutations in the fitness landscapes of an RNA and a protein. Nat Commun. 2023 Jun 19;14(1):3624.

29. Siltberg-Liberles J, Grahnen JA, Liberles DA. The Evolution of Protein Structures and Structural Ensembles Under Functional Constraint. Genes. 2011 Oct 28;2(4):748.

30. Halabi N, Rivoire O, Leibler S, Ranganathan R. Protein Sectors: Evolutionary Units of Three-Dimensional Structure. Cell. 2009 Aug 21;138(4):774–86.

31. Matange N, Bodkhe S, Patel M, Shah P. Trade-offs with stability modulate innate and mutationally acquired drug resistance in bacterial dihydrofolate reductase enzymes. Biochemical Journal. 2018 Jun 29;475(12):2107–25.

32. Rendel MD. Adaptive evolutionary walks require neutral intermediates in RNA fitness landscapes. Theoretical Population Biology. 2011 Feb 1;79(1):12–8.

33. Maes S, Deploey N, Peelman F, Eyckerman S. Deep mutational scanning of proteins in mammalian cells. Cell Reports Methods. 2023 Nov 20;3(11):100641.

34. Dunham AS, Beltrao P. Exploring amino acid functions in a deep mutational landscape. Molecular Systems Biology. 2021 Jul 22;17(7):e10305.

35. Saralamba N, Nakeesathit S, Mayxay M, Newton PN, Osorio L, Kim JR, et al. Geographic distribution of amino acid mutations in DHFR and DHPS in Plasmodium vivax isolates from Lao PDR, India and Colombia. Malaria Journal. 2016 Sep 21;15(1):484.

36. Park SC, Neidhart J, Krug J. Greedy adaptive walks on a correlated fitness landscape. Journal of Theoretical Biology. 2016 May 21;397:89–102.

37. Starr TN, Thornton JW. Epistasis in protein evolution. Protein Science : A Publication of the Protein Society. 2016 Feb 28;25(7):1204.

38. The UniProt Consortium. UniProt: the Universal Protein Knowledgebase in 2023. Nucleic Acids Research. 2023 Jan 6;51(D1):D523–31.

39. Yuan S, Chan HCS, Hu Z. Using PyMOL as a platform for computational drug design. WIREs Computational Molecular Science. 2017;7(2):e1298.

40. Fiser A, Do RK, Sali A. Modeling of loops in protein structures. Protein Sci. 2000 Sep;9(9):1753–73.

41. Eswar N, Webb B, Marti-Renom MA, Madhusudhan MS, Eramian D, Shen MY, et al. Comparative protein structure modeling using Modeller. Curr Protoc Bioinformatics. 2006 Oct;Chapter 5:Unit-5.6.

42. McGinnis S, Madden TL. BLAST: at the core of a powerful and diverse set of sequence analysis tools. Nucleic Acids Research. 2004 Jul 1;32(Web Server issue):W20.

43. Thompson JD, Higgins DG, Gibson TJ. CLUSTAL W: improving the sensitivity of progressive multiple sequence alignment through sequence weighting, position-specific gap penalties and weight matrix choice. Nucleic Acids Res. 1994 Nov 11;22(22):4673–80.

44. Strait BJ, Dewey TG. The Shannon information entropy of protein sequences. Biophysical Journal. 1996 Jul 1;71(1):148–55.

45. Gloor GB, Martin LC, Wahl LM, Dunn SD. Mutual Information in Protein Multiple Sequence Alignments Reveals Two Classes of Coevolving Positions. Biochemistry. 2005 May 1;44(19):7156–65.

46. Simonetti FL, Teppa E, Chernomoretz A, Nielsen M, Marino Buslje C. MISTIC: mutual information server to infer coevolution. Nucleic Acids Research. 2013 Jul 1;41(W1):W8–14.

47. Johnson DE, Xue B, Sickmeier MD, Meng J, Cortese MS, Oldfield CJ, et al. High-Throughput Characterization of Intrinsic Disorder in Proteins from the Protein Structure Initiative. Journal of structural biology. 2012 May 29;180(1):201.

48. Cui Q, Purisima EO, Wang E. Protein evolution on a human signaling network. BMC Syst Biol. 2009 Feb 18;3(1):21.

Supplemental Information

Navigating the Fitness Landscapes of Plasmodium falciparum Dihydrofolate Reductase: Evolutionary Insights into Antifolate Resistance

Danny Muzata[1,2#], Dwipanjan Sanyal[3#], Shivram A[1,2], Deeptanshu Pandey[4], Soumyananda Chakraborti[4], Aneesh S. Chivukula[2], Ravi Jasuja[5], Vladimir N. Uversky[6], Daniel Zielinski[7], Prajna D. Upadhyay[2], Mark Albers[8], and Sourav Chowdhury[5*]

Affiliations:
[1] One Health Trust, Bangalore, India
[2] Department of Computer Science and Information Systems, Birla Institute of Technology and Science-Pilani, Hyderabad, India.
[3] Structural Biology and Bioinformatics Division, CSIR-Indian Institute of Chemical Biology, Kolkata, India
[4] Department of Biological Sciences, Birla Institute of Technology and Science-Pilani, Hyderabad, India.
[5] Research Program in Men's Health: Aging and Metabolism, Brigham and Women's Hospital, Harvard Medical School, Boston, Massachusetts, USA
[6] USF Health Byrd Alzheimer's Research Institute, Morsani College of Medicine, University of South Florida, Tampa, FL 33612, USA
[7]Department of Bioengineering, University of California, San Diego, La Jolla, CA, USA
[8]Department of Neurology, Massachusetts General Hospital, Harvard Medical School, Boston, Massachusetts, USA

[*]Corresponding Author:

Sourav Chowdhury
Department of Biological Sciences,
Office: J Block-109,
Birla Institute of Technology and Science, Hyderabad Campus,
Hyderabad, Telangana, India, 500078
Email: sourav.chowdhury@hyderabad.bits-pilani.ac.in

[#]*These authors contributed equally to the work.*

Supplemental Figures

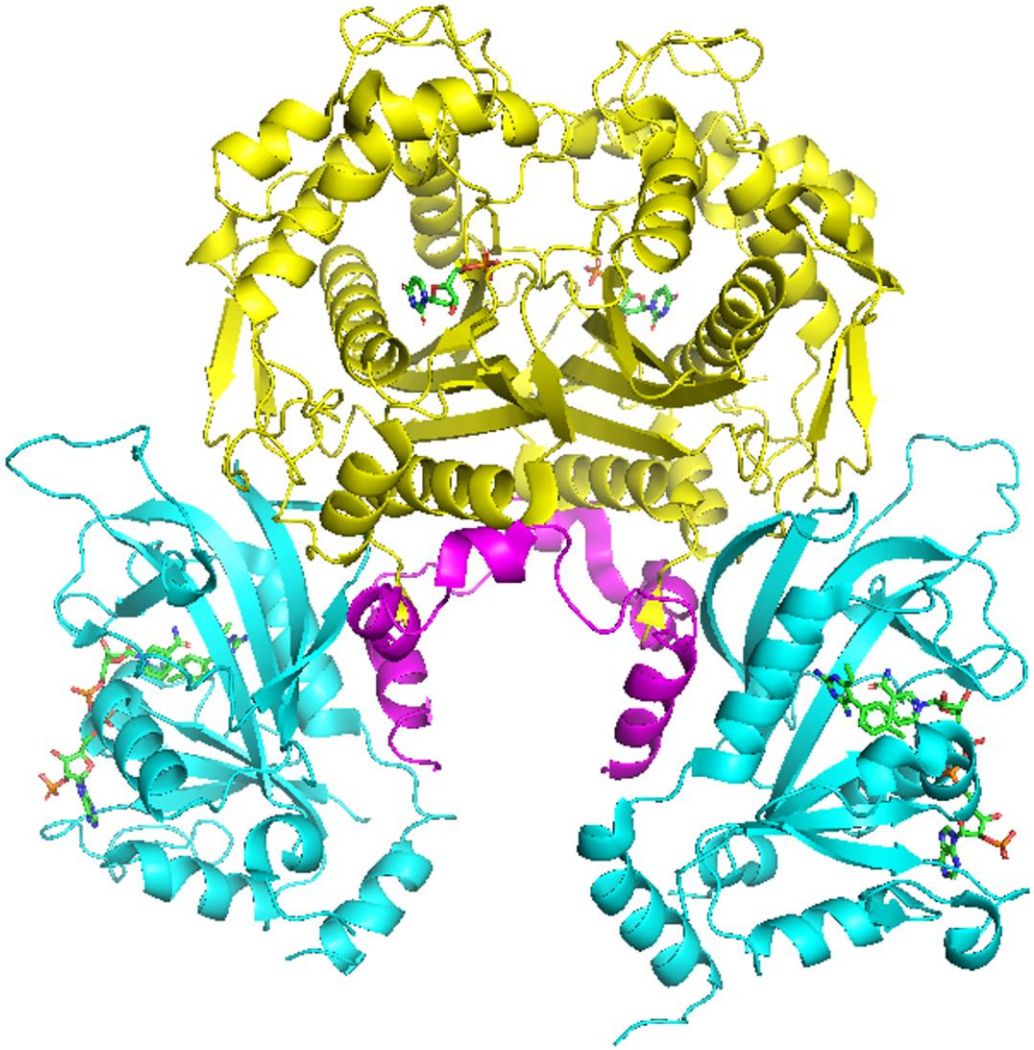

Supplemental Figure S1: This illustrates the 608 long *pf*DHFR-TS (PDB ID: 3QGT) dimeric assembly. In cyan are the DHFR domains with DHFR-TS junction in magenta and yellow region as TS domains. The DHFR domains are complexed with the drug pyrimethamine and NADPH cofactor

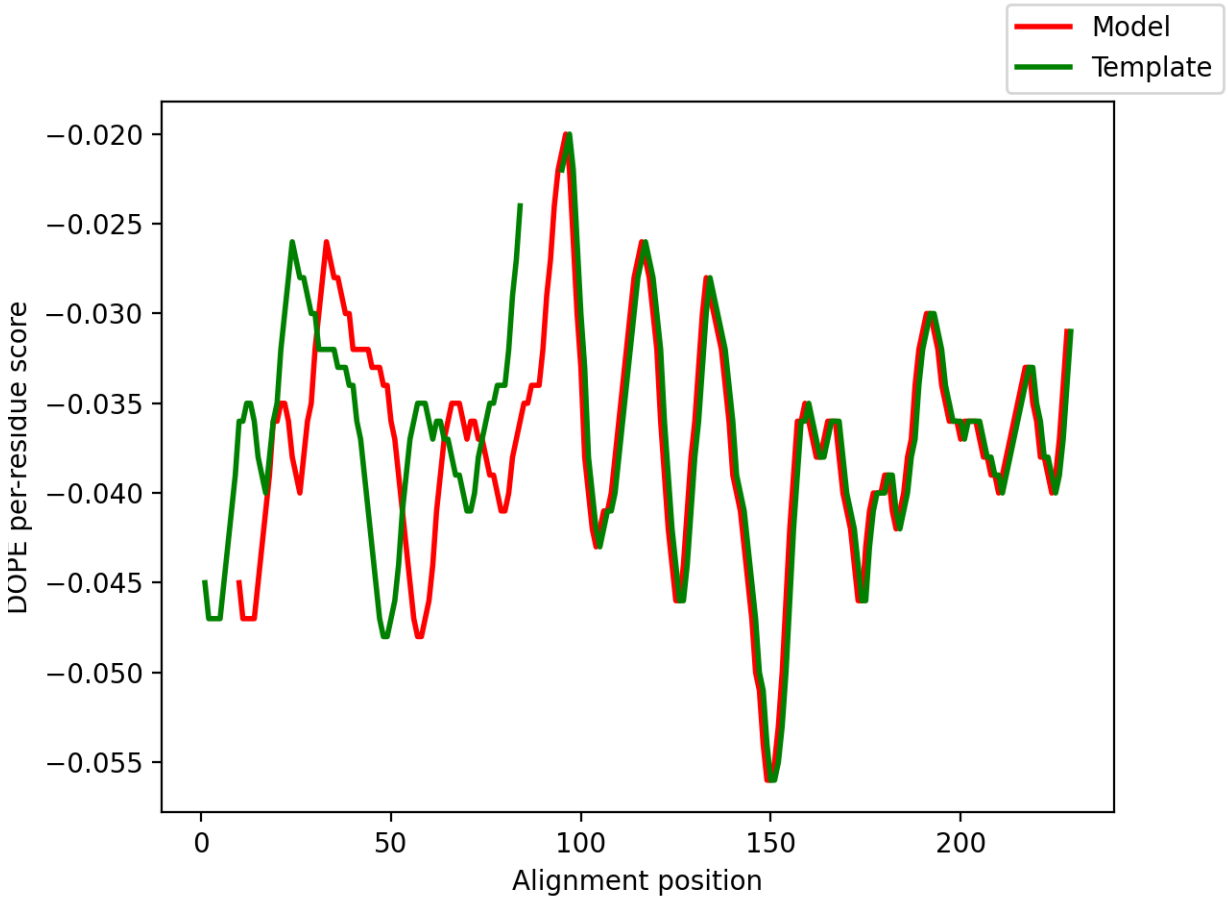

Supplemental Figure S2: This plot presents the validation results of homology modeling performed using Modeller. The DOPE scores for the model and template structures are compared across the alignment positions. The plot shows how well the model (red) aligns with the template (green). However, the misalignment observed between positions 0 to 96 is expected as it is due to the existing gap in the template structure.

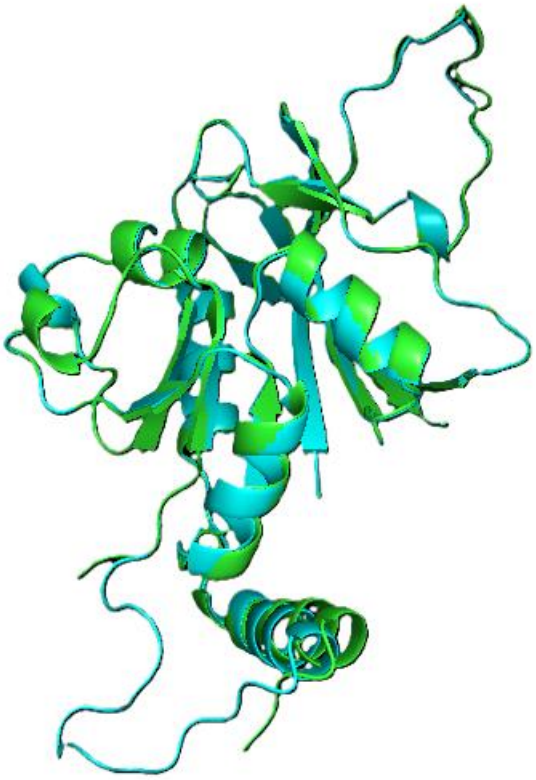

Supplemental Figure S3: Shows the structural alignment of the modeled DHFR domain (cyan) with the template structure (green) using PyMOL. The RMSD was calculated to assess the structural similarity between the model and the template. The RMSD value of 0.306 Å indicates a good alignment, validating the accuracy of the homology model. This alignment helps confirm that the modeled structure retains the key features and overall topology of the template.